Journal of the Korean Physical Society, Vol. 55, No. 4, October 2009, pp. 1720∼1723 Brief Reports

Secondary Electron Generation in Electron-beam-irradiated Solids: Resolution Limits to Nanolithography

Kyu Won Lee, S. M. Yoon, S. C. Lee, W. Lee, I.-M. Kim and Cheol Eui Lee*
Department of Physics and Institute for Nano Science, Korea University, Seoul 136-713

D. H. Kim
Seoul National University of Technology, Seoul 139-743

(Received 3 August 2009)

We have investigated the secondary electron generation in electron-beam-irradiated solids by means of a Monte Carlo simulation. The slow secondary electron energy was found to be independent of the position and the incident energy of the electron beam, and the electron beam broadening in thin films due to secondary electrons was found to be at least 5 – 10 nm, setting limits to the nanolithographic resolution.

PACS numbers: 79.20.Hx, 78.70.-g, 79.20.Ap
Keywords: Electron-beam nanolithography, Secondary electron generation, Monte Carlo simulation
DOI: 10.3938/jkps.55.1720

Electron scattering in solids plays a crucial role in electron-beam lithography and microscopy. The electron scattering processes in solids have been much studied, Monte Carlo simulations having made prominent achievements [1–3]. With the rapid growth of nanotechnology, the device feature size is approaching the region of secondary electrons. An early work employing a Monte Carlo simulation [4] showed that the ultimate resolution, taking the secondary electron effects into consideration in the electron-beam lithography of PMMA [poly(methylmethacrylate)], a representative resist material, is of the order of 10 nm. Since that pioneering work, Monte Carlo studies, including secondary electron generation and resist development, have been made [5–7]. However, most works have focused on the exposure profile and the resist development rather than on the the secondary electron generation itself, which is essential for higher lithographic resolution.

Two different types of secondary electrons may be considered: slow and fast secondary electrons with relatively low and high energies, respectively. Fast secondary electrons can travel large distances, which has the proximity effects. On the other hand, slow secondary electrons can travel, at best, several nanometers, forming an electron cloud around the primary electron beam and thus resulting in a beam broadening. The number of slow secondary electrons, which account for most secondary electrons, is known to be inversely proportional to the energy of the primary electrons in the high-energy region [6]. In this work, a Monte Carlo simulation was employed to gain a deeper insight into secondary electron generation.

In our Monte Carlo simulation of electron scattering, the screened Rutherford cross section was employed for elastic electron scattering [1], and the Gryzinski excitation function was used for the inelastic electron scattering with core and valence electrons [1, 8]. A single secondary electron with energy $E_S = \Delta E - E_b$ was generated for each inelastic scattering, ΔE and E_b being the energy lost by the primary electron and the binding energy of the core or the valence electron, respectively.

Electron beams with an incident energy of E_o and with a square cross section of 1 nm × 1 nm were injected along the z axis perpendicular to the sample surface (x-y plane). The position, energy, and scattering angle of the secondary electrons generated were used as the initial conditions for the simulation of the secondary electron trajectories, which were traced down to the cutoff energy of 20 eV. Only the first generation of secondary electrons with an energy E_S larger than 10 eV was considered; cascade generation was excluded.

The distribution functions $f(x_n)$ and $f(z_n)$ of the electron hits and energy, where $x_n = z_n = nL$, with n being an integer, was constructed along the x or z axis by counting the electron hits and energy in each division with a length of $L = 1$ nm. The mean broadening,

$$< x_n >= \frac{\sum x_n f(x_n)}{\sum f(x_n)}, \qquad (1)$$

was thus calculated. The mean broadening, being uniaxial about the z axis, was taken to be the half-width. Thus, the mean broadening of an electron beam of 1 nm

*E-mail: rscel@korea.ac.kr; Fax: +82-2-927-3292

Table 1. Mean binding energy (eV) of the core (E_{core}) and the valence electrons (E_{vale}) per atom [4,9].

	E_{core}	E_{vale}
PMMA	408	10.5
Si	112	8

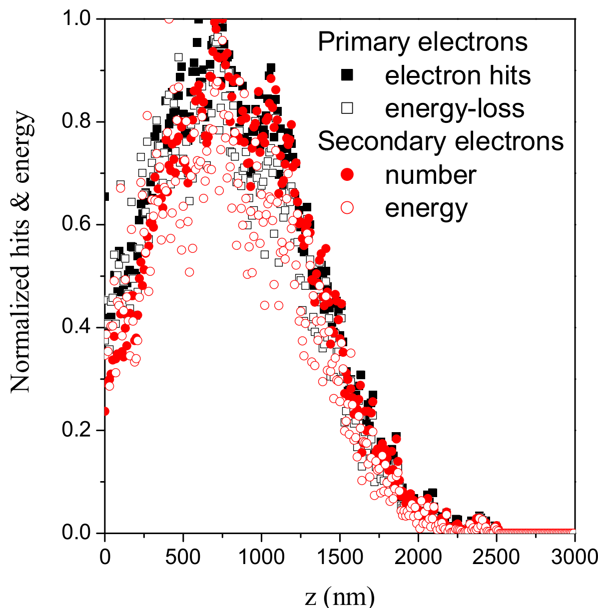

Fig. 1. Normalized distributions of the hits and the energy loss of primary electrons are shown along with the normalized distributions of the generation number and of the energy of secondary electrons along the z axis in a PMMA bulk.

× 1 nm is 0.5 nm. Mean binding energies per atom, as shown in Table 1, were used [3,9].

Figure 1 shows the normalized distributions of the hits and the energy loss of the primary electrons along with the normalized distributions of the generation number and the energy of the secondary electrons along the z axis in a PMMA bulk irradiated with 1000 electrons of E_o = 10 keV. The z axis was divided into divisions of 10 nm in length. In each division, the electron hits and the energy loss of the primary electrons, as well as the generation number and the energy of the secondary electrons, were counted and normalized so that their maximum values were unity. All four quantities collapsed onto a single curve, indicating that the mean energy loss of the primary electrons and the mean secondary electron energy generated are nearly independent of the position. The secondary electron energy turns out to be proportional to the energy loss of the primary electron, which may readily be understood.

The mean energy of the secondary electrons generated may simply be defined as the total energy divided by the total secondary electron generation number, the mean energy being independent of position, as shown in Fig. 1.

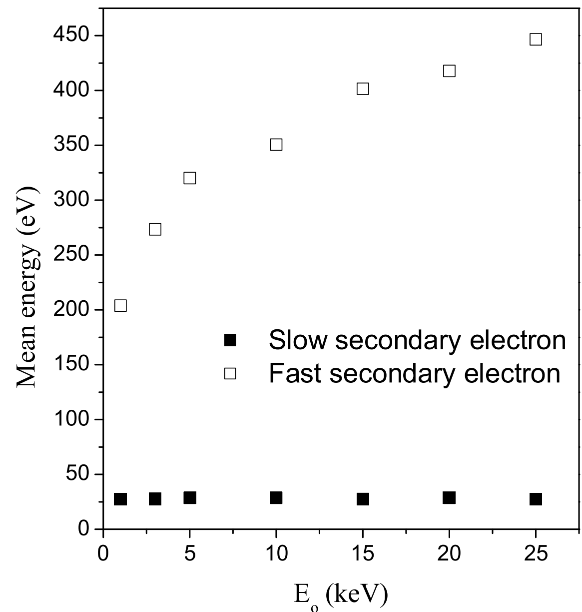

Fig. 2. Mean energies of slow (solid squares) and fast (open squares) secondary electrons as functions of the incident energy E_o of the electron beam in a PMMA bulk.

The secondary electron generation number is roughly inversely proportional to the square of the secondary electron energy [6]. In this work, secondary electrons with energies of 10 to 100 eV were considered to be the slow secondary electrons, and fast secondary electrons were taken to have energies higher than 100 eV.

Figure 2 shows the mean energies of slow and fast secondary electrons as functions of the electron beam incidence energy E_o in a PMMA bulk irradiated with 1000 electrons. The secondary electron generation number, as shown in Fig. 3, is linearly proportional to E_o. The mean energy of the fast secondary electrons increases with increasing E_o, higher-energy primary electrons being able to produce higher-energy secondary electrons. Interestingly enough, the mean energy of the slow secondary electrons is found to be independent of E_o. The facts that the secondary electron energy determines the distance travelled and that the mean secondary electron energy is independent of E_o and position would impose an intrinsic limitation on external control of the electron beam broadening.

Figure 4 shows the mean broadening of primary and secondary electrons as functions of the incident energy E_o in a 100-nm-thick PMMA film. In order to exclude the backscattering effect from the substrate, the PMMA film was considered to stand alone in vacuum. More incident electrons had to be introduced for the simulation of higher incident energies, the secondary electron generation number decreasing with increasing E_o in a thin film [6]. The mean broadening of the primary electrons, showing a rapid decrease with increasing incident energy

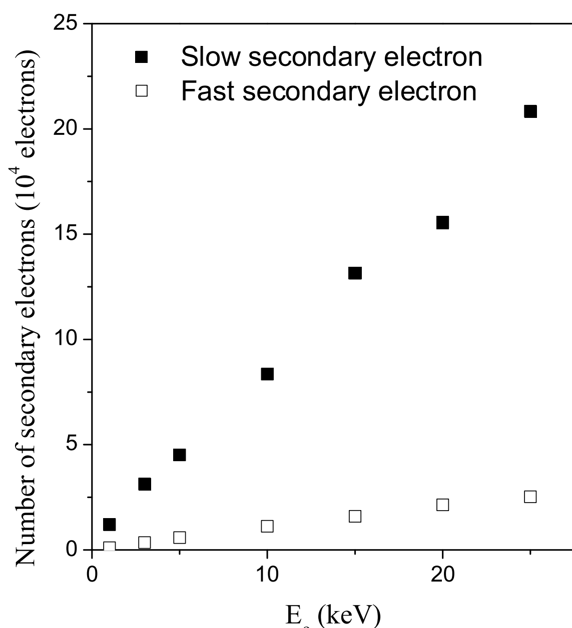

Fig. 3. Generation number of slow (solid symbols) and fast secondary electrons (open symbols) as functions of the incident energy E_o in a PMMA bulk.

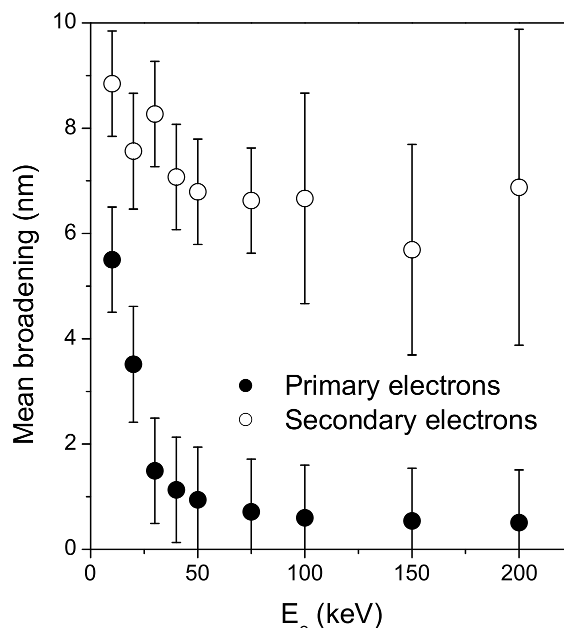

Fig. 4. Mean broadening of primary (solid symbols) and secondary electrons (open symbols) as functions of the incident energy E_o in a PMMA thin film.

up to 50 keV, is about the electron beam size at energies above 100 keV, indicating no beam broadening due to the primary electrons. The mean broadening of the secondary electrons decreased only slightly with increasing incident energy, staying at around 6 – 7 nm even up to the highest energy of 200 keV. The secondary electrons, thus, impose an eventual restriction on the lithographic resolution in thin films.

Figure 5 shows the mean broadening of primary and secondary electrons as functions of E_o in a PMMA(100 nm)/Si film, in which electrons backscattered from the Si substrate give rise to a much enhanced beam broadening. As was the case in a PMMA free-standing film (Fig. 4), the mean broadening of both primary and secondary electrons shows a rapid decrease with increasing E_o up to about 50 keV. Besides, while the mean broadening of primary electrons keeps decreasing slowly with increasing E_o even at energies above 50 keV, that of secondary electrons stays at around 5 – 10 nm, as was the case in a free-standing film (Fig. 4).

Most secondary electrons (∼90 %) were slow secondary electrons whose mean energy of 28 eV was independent of incident energy (Figs. 2 and 3). Most of secondary electrons generated by cascade generation had energies lower than 10 eV, for which the travelled distance was, at best, 1 nm, so they were not considered in this work. Cascade generation, in fact, does not have a significant effect on the number of secondary electrons generated or on the mean broadening.

In summary, a Monte Carlo simulation was employed to study secondary electron generation in solids irradiated with electron beams. The mean energy of slow secondary electrons was revealed to be independent of position and of the electron beam incident energy. The beam broadening due to secondary electrons was shown not to go below 5 – 10 nm even at high electron beam energies,

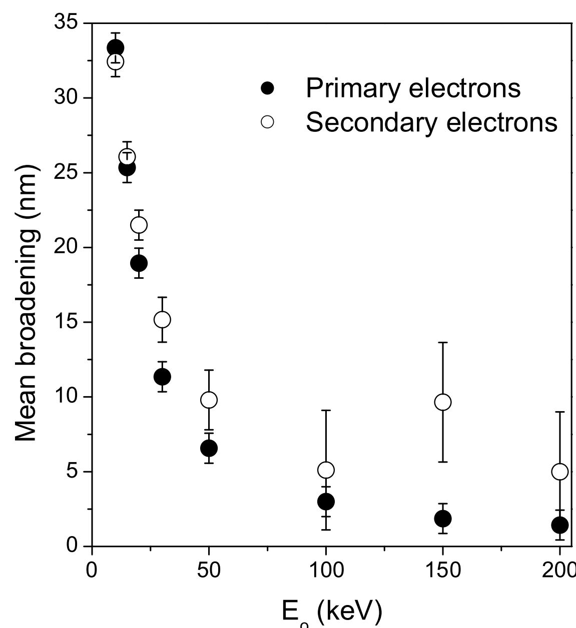

Fig. 5. Mean broadening of primary (solid symbols) and secondary electrons (open symbols) as functions of the incident energy E_o in a PMMA(100 nm)/Si thin film.

setting a resolution limit on nanolithography.

ACKNOWLEDGMENTS

This work was supported by the Seoul Research and Business Development Program (Grant No. 10583) and by the Korea Ministry of Education, Science and Technology (NRL Program R0A-2008-000-20066-0, User Program of Proton Engineering Frontier Project, No. 20090082672).

REFERENCES

[1] R. Shimizu and D. Ze-Jun, Rep. Prog. Phys. **55**, 487 (1992).
[2] R. Shimizu, Y. Kataoka, T. Ikuta, T. Koshikawa and H. Hashimoto, J. Phys. D: Appl. Phys. **9**, 101 (1976).
[3] S. Valkealahti and R. M. Mieminen, Appl. Phys. A **32**, 95 (1983); I.-H. Oh, J. J. Kweon, B. H. Oh and C. E. Lee, J. Korean Phys. Soc. **53**, 3497 (2008).
[4] N. Samoto and R. Shimizu, J. Appl. Phys. **54**, 3855 (1983).
[5] M. Aktary, M. Stepanova and S. K. Dew, J. Vac. Sci. Technol. B **24**, 768 (2006).
[6] B. Wu and A. R. Neureutherb, J. Vac. Sci. Technol. B **19**, 2508 (2001).
[7] M. Yasuda, T. Nobuo and H. Kawata, Jpn. J. Appl. Phys. **43**, 4004 (2004); Y. H. Lee, I. H. Oh, K. W. Lee, S. M. Yoon and C. E. Lee, J. Korean Phys. Soc. **51**, 1457 (2007).
[8] M. Gryzinski, Phys. Rev. **138**, 336 (1965).
[9] J. A. Bearden and A. F. Burr, Rev. Mod. Phys. **39**, 125 (1967).